Supporting Information:

Exciplex Formation in Bimolecular Photoinduced Electron Transfer Investigated by Ultrafast Time-Resolved Infrared Spectroscopy

Marius Koch, Romain Letrun, and Eric Vauthey[1]

Department of Physical Chemistry, University of Geneva, 30 quai Ernest-Ansermet, CH-1211 Geneva, Switzerland

Email: eric.vauthey@unige.ch Content

Content

[1] To whom correspondence should be addressed

1 Procedures

1.1 Chemicals

9-Cyanoanthracene (CA, Sigma-Aldrich, 97%), phthalic anhydride (PA, Sigma-Aldrich, >99%) and dicyanoethylene (DCE, Fluka, >98%) were purified by sublimation before use. 3-Cyanoperylene (CNPE) and 3-methylperylene (MEPE) were synthesized according to the literature,[S1] and purified by column chromatography. Acetonitrile (ACN, Fisher) and tetrahydrofuran (THF, Acros Organics) were of the highest spectroscopic purity and used as received.

1.2 Spectroscopy

1.2.1 Steady-State Measurements.

Absorption spectra were recorded on a Cary 50 spectrophotometer and the fluorescence spectra were measured on a Cary Eclipse fluorimeter (step size: 75 cm^{-1}, excitation slit: 2.5 nm, emission slit: 2.5 nm). The experiments were carried out in a 10 mm quartz cuvette. The steady-state IR absorption spectra were recorded in KBr pellets using a Bio Rad (Excalibur Series) FTIR Spectrometer with a resolution of 2 cm^{-1}.

1.2.2 Time-Resolved Fluorescence.

Sub-nanosecond time-resolved fluorescence decays were measured using the time-correlated single photon counting (TCSPC) technique with the setup described in reference S2. Briefly, excitation was performed with a laser diode at 395 nm (Picoquant model LHD-P-C-400B) for CA and MEPE and at 470 nm (Picoquant model LHD-D-C-470) for CNPE. The pulse duration of both diodes was 60 ps. The full width at half maximum (FWHM) of the instrument response function was about 200 ps. Linearly polarized excitation was ensured by passing the excitation beam through a Glan-Taylor polarizer. The emission was collected at magic angle after passing trough an interference filter of 8 nm bandwidth at 450 nm for CA and MEPE and of 9 nm bandwidth at 520 nm for CNPE. The absorbance of all sample solutions was below 0.07 at the excitation wavelength in a 10 mm quartz cuvette.

1.2.3 Transient Electronic Absorption.

Femtosecond transient electronic absorption spectra were obtained using an apparatus described in references S3. The instrument response function had a FWHM of approximately 200 fs as obtained from measurements of the optical Kerr effect in ACN. The pump pulse energy at 400 nm was 1 μJ, resulting in an irradiance of about 1 mJ/cm^2 on the sample. The sample absorbance at 400 nm was < 0.5 in a 1 mm quartz cuvette. Samples were bubbled with nitrogen during the experiment to constantly refresh the excitation volume, thus avoiding sample decomposition. No changes were observed throughout the experiments. All experiments were carried out at magic angle (54.7°).

1.2.4 Transient Vibrational Absorption.

Femtosecond transient vibrational absorption spectra were obtained with the setup described in reference S4 and based on a Ti:Sapphire amplified system (Spectra Physics Solstice) producing 100 fs pulses at 800 nm at 1 kHz. Excitation was performed with a 2 μJ

pulse at 400 nm produced by frequency doubling of a fraction of the amplifier output. The polarization was controlled with a Glan-Laser polarizer, limiting the time resolution of the experiment to 300 fs. The pulses were focused on the sample to a spot of 350 μm resulting in an irradiance of 1.9 mJ/cm^2. Mid-IR probe pulses at around 4.6 μm (C≡N) and 5.7-7 μm (C=C and C=O) where generated by difference frequency mixing of the output of an optical parametric amplifier (Light Conversion, TOPAS-C with NDFG module) that was pumped at 800 nm. The polarization of the IR beam was controlled using a wire-grid polarizer. Two horizontally polarized IR beams were produced with a CaF_2 wedge and focused onto the sample to a 140 μm diameter spot. One of the beams was overlapped with the pump beam, whereas the second one was used as a reference. Both IR beams were focused onto the entrance slit of an imaging spectrograph (Horiba, Triax 190, 150 lines/mm) equipped with a liquid nitrogen cooled 2 x 64 element MCT array (Infrared Systems Development), giving a resolution of 3-4 cm^{-1} (C≡N) and 1-2 cm^{-1} (C=C, C=O).

The sample area and the detection system were placed in a box that was purged with dry air for at least 45 minutes before each experiment. The average of 3000 signal shots was taken to collect one data point with the polarization of the pump parallel to that of the IR pulse. After measuring over the entire temporal window, the experiment was repeated with the polarization of the pump perpendicular to that of the IR pulse. This procedure was carried out for at least eight times for each polarization. To provide a new sample solution for each shot, a flow cell as described in reference S5 was used. The absorbance at 400 nm was below 0.3 on a 100 μm optical pathlength (on 200 μm for CNPE/PA in ACN). The wavenumber axis was calibrated by comparing the bleach of the C=C and C≡N stretching bands of the donors used with the steady-state absorption spectra measured using the FTIR spectrometer. No significant sample degradation was observed throughout the experiment. To avoid changes due to the evaporation of THF during the experiment, the sample solution was 10 mL.

Given the bandwidth of the IR pulses (400 nm), transient spectra recorded in four, resp. two, ca. 100-150 cm^{-1} spectral windows were merged to cover the 1500-1750 cm^{-1} and 2100-2220 cm^{-1} spectral regions.

All data sets at the same polarization were first compared to detect possible problems during the measurements. The spectra were then averaged and the different windows merged to obtain a single spectrum for each polarization. The resulting spectra recorded at both polarizations were then compared, and regions without signal were inspected to identify the baseline. The baseline was set to zero and the anisotropy calculated. No tail matching had to be carried out.

1.3. Global Data Analysis

The procedure followed for global target analysis of the data recorded with CA and 1M PA in THF can be decomposed in three steps:

1) The amplitudes of time profiles of the LE, EX, IP and depleted GS bands were scaled to reflect the actual populations, *N*, assuming that the sum of these populations should be constant in time and centered around zero, i.e. $N_{LE}(t)+N_{EX}(t)+N_{IP}(t)=-N_{GS}(t)$. This was done as follow:

- N_{GS}: At early time delays (t < 10 ps), the intensity of the GS bleach signal remains constant and is the strongest. The corresponding time profile was therefore scaled so that the average intensity at time delays < 10 ps was equal to -1.
- N_{LE}: The time profile was not scaled to 1 at the earliest time delay, as it would be the case if all the population was in the local excited state, but to 0.97, to account for the small amount of exciplex already present at 1 ps (Figure 5B main text, positive signal at 1682 cm^{-1}).
- N_{EX}/N_{IP}: The relative extinction coefficients of the EX and IP bands were estimated by comparing the intensity of the transient bleach band and the LE and $PA^{\cdot -}$ bands measured with the CA/PA and MEPE/PA pairs upon identical excitation conditions, considering that the depleted ground-state population, N_{GS}, that is not in the LE state is entirely the IP state (MEPE/PA) or in either IP or EX states (CA/PA). The resulting scaled time profiles at 1616 cm^{-1} and 1682 cm^{-1} (Figure 7 main text) show that, at about 500 ps, $N_{EX} \approx N_{IP}$.

2) A given reaction scheme, e.g. Scheme 1, was fit to the scaled time profiles using an iterative nonlinear least-squares fitting procedure based on the trust region reflective algorithm,[S6] yielding a set of time constants. During this step, the initial population of a given species was fixed and taken as the respective intensity of the first data point, i.e. $N_{LE}(t=1ps)=0.97$, $N_{EX}(t=1ps)=0.03$, $N_{IP}(t=1ps)=0$, $N_{GS}(t=1ps)=-1$, thus leaving the time constants as the sole variables to optimize.

3) In the last step, the transient spectra measured in both the 1500-1750 cm^{-1} and 2100-2220 cm^{1} spectral windows were merged and fit to the same model that was used in Step 2, using the time constants previously obtained as fixed parameters. The global target analysis procedure is based on a routine using a combination of an initial value ordinary differential equation solver and the matrix reconstruction algorithm.[S7] The optimization was performed iteratively with the Nedler-Mead algorithm.

The whole procedure described here has been performed using MATLAB (The MathWorks Inc.), using its implementation of the various algorithms cited, except for the matrix reconstruction algorithm that we implemented ourselves.

1.4. Quantum Chemistry Calculations

Ground-state gas phase geometry optimization and frequency calculations were performed at the density functional level of theory (DFT) using the B3LYP functional and the 6-31G(d) basis set. No scaling factor was used to correct the vibrational frequencies. The calculations were carried out using the Gaussian 09 package.[S8]

2 Data

2.1. Steady-State Fluorescence

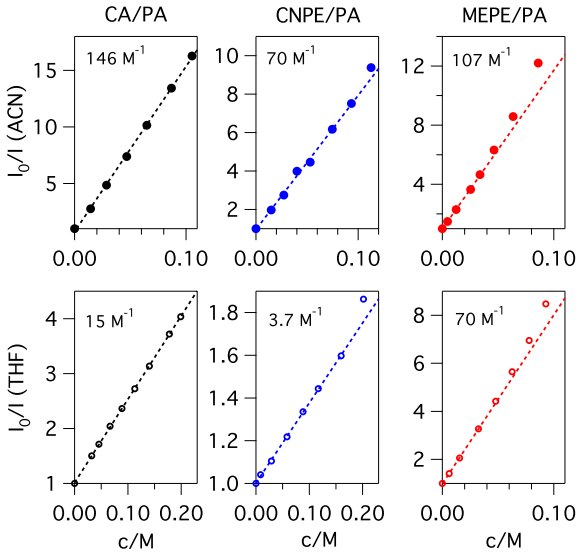

Figure S1. Stern-Volmer (SV) plots of the fluorescence quenching of the donors by PA in ACN (top) and THF (bottom). The dotted lines are linear fits to the data. A positive curvature is observable for the MEPE/PA pair (larger driving force) due to the transient effect. Therefore, only data at concentrations < 0.05 M were used for the SV-analysis. Since quenching is slower than diffusion for the two other D/A pairs, the transient effect is not very pronounced (CNPE/PA) or negligible (CA/PA) at low concentrations.

Table S1. Results from the SV-analysis of the three D/A pairs in ACN and THF. τ_f is the excited-state lifetime of the donor in the absence of quencher obtained from TCSPC measurements, K_{SV} the SV constant obtained from a linear fit to the SV plots, k_q the quenching rate constant and k_{diff} the diffusion rate constant calculated as $k_{diff} = \frac{8 \cdot 10^6 RT}{3\eta}$, with R the molar gas constant, T the temperature and η the viscosity in cP.

		τ_f /ns, [PA] = 0	K_{SV} /M^{-1}	k_q /10^9 M^{-1}s^{-1}	k_{diff} /10^9 M^{-1}s^{-1}
CA/PA	ACN	11.4	146	12.8	17.9
	THF	10.6	15	1.4	14.4
CNPE/PA	ACN	5.1	70	13.7	17.9
	THF	4.8	3.7	0.8	14.4
MEPE/PA	ACN	4.2	107	25.5	17.9
	THF	4.1	70	17.1	14.4

2.2. Time-Resolved Fluorescence

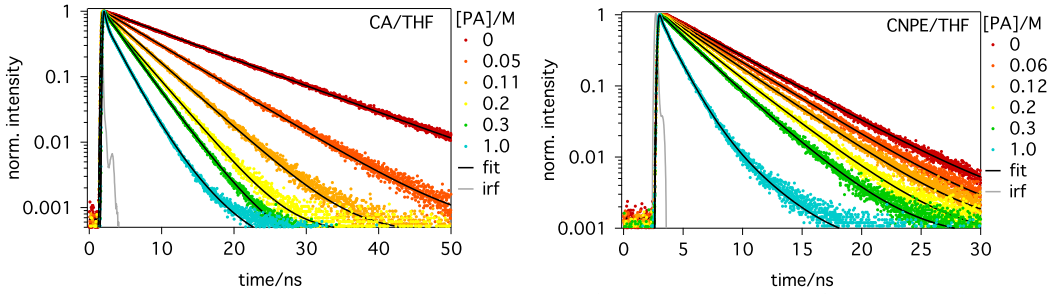

Figure S2. Fluorescence time profiles measured with CA (left, 395 nm excitation) and CNPE (right, 470 nm excitation) with different PA concentrations in THF.

2.3. Transient Electronic Absorption

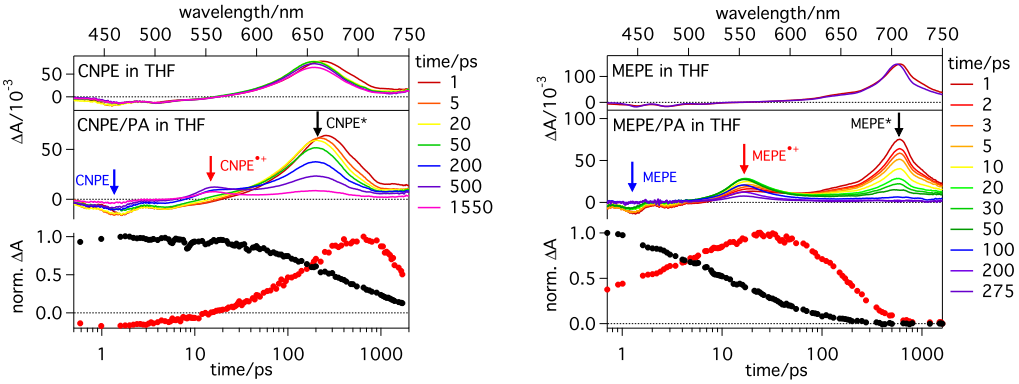

Figure S3. Transient electronic absorption spectra measured in THF at various time delays after excitation of CNPE (left) and MEPE (right) without PA (top) and in the presence of 1M PA (middle). Bands ascribed to excited-state absorption, ground-state bleach, and radical cation are indicated by the arrows. The temporal profiles of the excited-state absorption (black) and the cation (red) in the presence of PA are also shown (bottom).

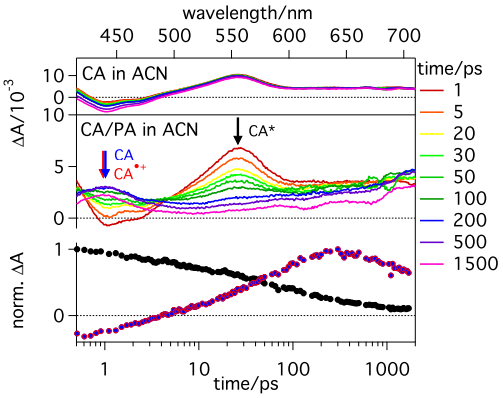

Figure S4. Transient electronic absorption spectra measured at various time delays after excitation of CA without PA (top) and in the presence of 1M PA (middle) in ACN. The temporal profiles at the wavelengths shown by arrows are also shown (bottom).

2.4. Quantum Chemistry Calculations

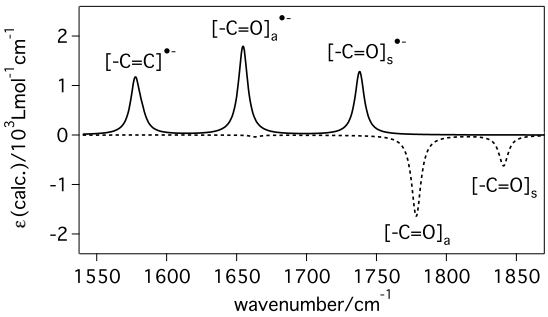

Figure S5. Calculated IR absorption spectra of PA·⁻ (solid line) and PA (dashed line, multiplied by -1) in the C=C and C=O stretching region.

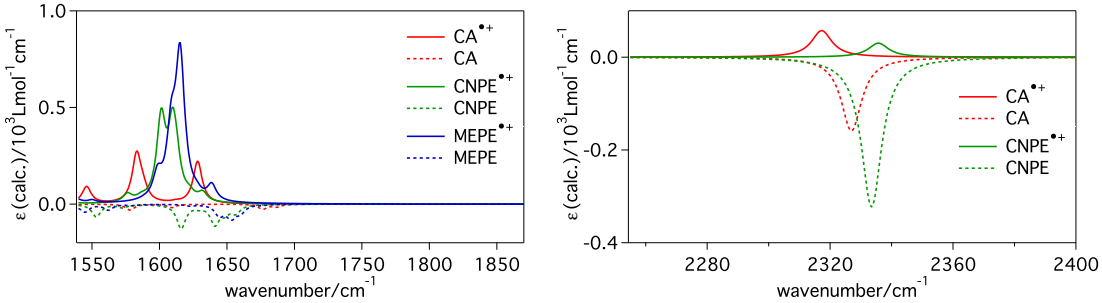

Figure S6. Calculated IR absorption spectra of the donor radical cations (solid lines) and donors in the ground state (dashed lines, multiplied by -1) in the C=C (left) and C≡N (right) stretching regions.

2.5 Transient Vibrational Absorption.

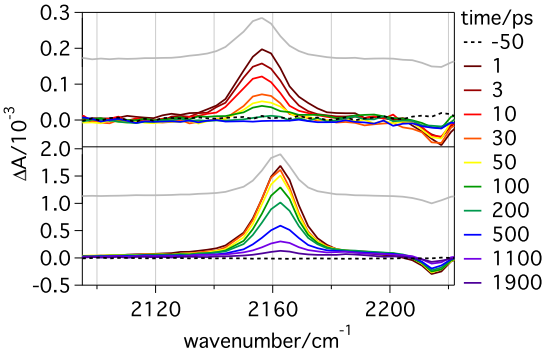

Figure S7. Transient IR spectra measured at several time delays after 400 nm excitation of CNPE with 1M PA in ACN (top) and THF (bottom). As a comparison, spectra measured 1 ps after excitation of CNPE alone are also shown (grey).

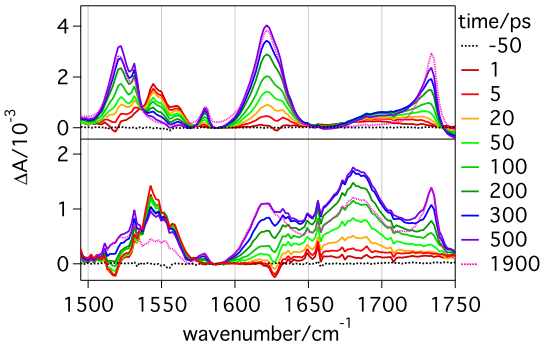

Figure S8. Transient IR spectra measured at several time delays after 400 nm excitation of CA with 0.2M PA in ACN (top) and THF (bottom).

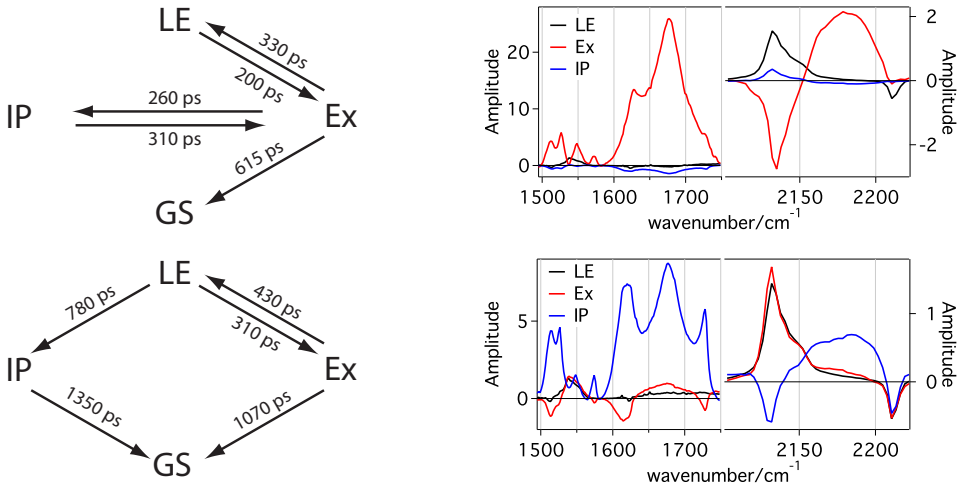

Figure S9. (Left) Alternative target models reproducing satisfactorily the kinetics shown in Figure 7 (main text) and (Right) resulting species-associated difference spectra obtained using the time constants in the left panels as fixed parameters.

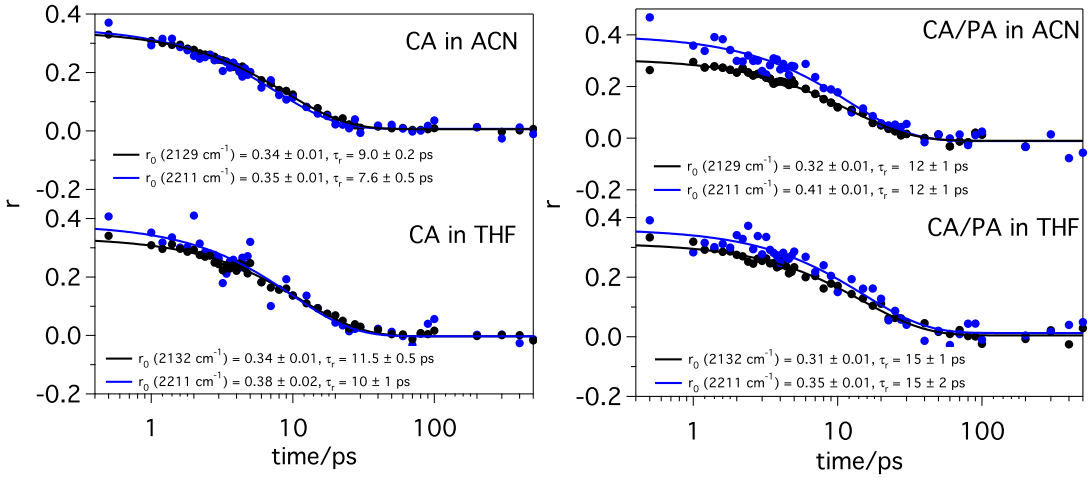

Figure S10. Anisotropy decays of the C≡N stretching band of CA* (black) and CA (blue) without (left) and with 1M PA (right) in ACN and THF, and best exponential fits (solid lines).

2.5 Steady-State Vibrational Absorption

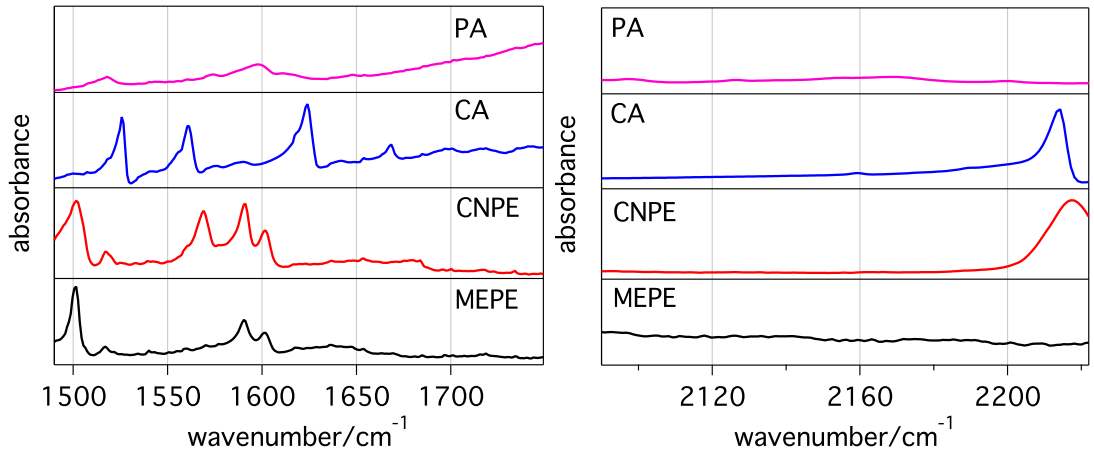

Figure S11. FTIR absorption spectra in the C=O, C=C (left) and C≡N regions (right) measured with PA, CA, CNPE and MEPE in KBr.

3 References

(S1) Buu-Hoï, N. P.; Long, C. T. *Rec. Trav. Chim. Pays-Bas* **1956**, *75*, 1221.
(S2) a) Muller, P.-A.; Högemann, C.; Allonas, X.; Jacques, P.; Vauthey, E. *Chem. Phys. Lett.* **2000**, *326*, 321; b) Fürstenberg, A.; Vauthey, E. *Photochem. Photobiol. Sci.* **2005**, *4*, 260.
(S3) a) Duvanel, G.; Banerji, N.; Vauthey, E. *J. Phys. Chem. A* **2007**, *111*, 5361; b) Banerji, N.; Duvanel, G.; Perez-Velasco, A.; Maity, S.; Sakai, N.; Matile, S.; Vauthey, E. *J. Phys. Chem. A* **2009**, *113*, 8202.
(S4) Koch, M.; Rosspeintner, A.; Adamczyk, K.; Lang, B.; Dreyer, J.; Nibbering, E. T. J.; Vauthey, E. *J. Am. Chem. Soc.* **2013**, *135*, 9843.
(S5) Bredenbeck, J.; Hamm, P. *Rev. Sci. Instrum.* **2003**, *74*, 3188.
(S6) Conn, A. R.; Gould, N. I. M.; Toint, P. L. *Trust-Region Methods*; Society for Industrial and Applied Mathematics: Philadelphia, 1987.
(S7) Fita, P.; Luzina, E.; Dziembowska, T.; Radzewicz, C.; Grabowska, A. *J. Chem. Phys.* **2006**, *125*, 184508.
(S8) Frisch, M. J.; Trucks, G. W.; Schlegel, H. B.; Scuseria, G. E.; Robb, M. A.; Cheeseman, J. R.; Scalmani, G.; Barone, V.; Mennucci, B.; Petersson, G. A.; Nakatsuji, H.; Caricato, M.; Li, X.; Hratchian, H. P.; Izmaylov, A. F.; Bloino, J.; Zheng, G.; Sonnenberg, J. L.; Hada, M.; Ehara, M.; Toyota, K.; Fukuda, R.; Hasegawa, J.; Ishida, M.; Nakajima, T.; Honda, Y.; Kitao, O.; Nakai, H.; Vreven, T.; Montgomery Jr., J. A.; Peralta, J. E.; Ogliaro, F.; Bearpark, M.; Heyd, J. J.; Brothers, E.; Kudin, K. N.; Staroverov, V. N.; Kobayashi, R.; Normand, J.; Raghavachari, K.; Rendell, A.; Burant, J. C.; Iyengar, S. S.; Tomasi, J.; Cossi, M.; Rega, N.; Millam, J. M.; Klene, M.; Knox, J. E.; Cross, J. B.; Bakken, V.; Adamo, C.; Jaramillo, J.; Gomperts, R.; Stratmann, R. E.; Yazyev, O.; Austin, A. J.; Cammi, R.; Pomelli, C.; Ochterski, J. W.; Martin, R. L.; Morokuma, K.; Zakrzewski, V. G.; Voth, G. A.; Salvador, P.; Dannenberg, J. J.; Dapprich, S.; Daniels, A. D.; Farkas, Ö.; Foresman, J. B.; Ortiz, J. V.; Cioslowski, J.; Fox, D. J. *Gaussian 09 (revision A1);* Wallingford, CT, 2009.